Engineering and Applied Science Letters

PSR Press

Article

Synthesis and characterization of biopolymer-based fire-retardant coatings for thermal insulation in low-cost buildings and industrial plants

C.S. Onyima[1,*], O. Eyide[2], J. C. Mbah[2], D. N.Onwenna[2] and N. A. Ozioma[3]

[1] Alpha Research Laboratory, Awka, Anambra, State, Nigeria
[2] Department of Chemical Engineering, University of Delta, Agbor, Delta State, Nigeria
[3] Department of Renewable Energy Technology, Federal Polytechnic Orogun, Delta State, Nigeria
* Correspondence: odeworitse.eyide@unidel.edu.ng

Received: 08 November 2025; Accepted: 20 March 2026; Published: 30 March 2026.

Abstract: This study reports the synthesis of a sustainable biopolymer-based coating using cassava starch as the polymeric matrix, oil-palm empty fruit bunch (EFB) lignin as reinforcement, and acid-activated nano-bentonite clay with boric acid as a crosslinker. Coatings were applied to mild-steel substrates and characterized using FTIR, TGA, SEM/TEM, XRD, BET, thermal conductivity measurements, and ASTM E1321 lateral ignition and flame-spread tests. FTIR confirmed hydrogen bonding and strong interfacial adhesion, indicated by O–H and C=O stretching from borate crosslinking, aromatic C=C (lignin), and Si–O–Si (bentonite) vibrations, with an O–H peak shift from 3405 to 3378 cm^{-1}. TGA revealed three-stage decomposition with increased onset degradation temperature (300 °C) and enhanced char yield (27.5%). SEM/TEM showed well-dispersed bentonite nanoparticles (<100 nm) and dense post-burn char morphology, while XRD indicated partial intercalation/exfoliation of clay, and BET confirmed increased surface area and mesoporosity. Optimized formulations (Sample B) exhibited superior fire performance: ignition delay of 126 ± 4 s, flame-spread rate of 1.0 ± 0.1 cm min^{-1}, and char continuity of 92 ± 3%, alongside a 35–45% reduction in thermal conductivity. Mechanical evaluations demonstrated improved adhesion, abrasion resistance, and hydrophobicity. These findings confirm that multi-component, bio-based coatings derived from locally available materials provide a low-cost, eco-friendly strategy for fire retardancy and thermal insulation, supporting sustainable development goals (SDGs 9, 11, and 13).

Keywords: biopolymer coating, thermal insulation, lignin, starch, nano-bentonite

1. Introduction

Fire remains one of the most destructive hazards for both residential and industrial built environments worldwide. In low-cost housing and resource-constrained industrial facilities the protection systems, and limited access to rapid emergency response [1]. Beyond immediate loss of life and property, fires precipitate prolonged disruption to livelihoods, local economies and essential services; they also release large quantities of toxic combustion products that harm indoor air quality and human health [2]. The International Energy Agency (IEA) has stated that global energy consumption is expected to rise by 53% over the next decade. This will contribute to the growth in industrial and prompt urbanization as a result of increase in population size leading to infrastructure development [3]. According to the IEA report in 2022, 34% of global energy consumption accounts for building operations, which indicates around one-third of global energy consumption where 20% includes sole energy consumption by electricity and heat used in the buildings, and around 10% indicates direct energy emission by the building [4,5]. Reliable, low-cost strategies that reduce flammability and slow heat transfer are therefore central to improving fire safety and thermal performance in these contexts.

Historically, fire protection of structural and finishing materials has relied on halogenated flame retardants, intumescent coatings based on petroleum-derived binders, and inorganic fillers such as aluminum hydroxide and ammonium polyphosphate. While effective, many conventional systems suffer from

environmental or health concerns, high cost, limited local availability, and poor end-of-life disposal characteristics [6]. The pressing need for affordable, safe, and sustainable building materials has intensified in recent years, particularly in the context of low-cost housing and industrial infrastructure in emerging economies. Fire safety and thermal performance are critical parameters in construction materials making the development of biopolymer-based fire-retardant coatings a favorable research solution.

Biopolymers such as starch have attracted considerable attention due to their renewability, biodegradability, and potential for modification either by cross-linking or reinforcement to tailor thermal and mechanical properties [7]. Cassava (*Manihot esculenta* Crantz) is a major source of starch in tropical regions; cassava starch has been widely used in food, packaging and biodegradable plastics research and is increasingly investigated as a component of functional coatings due to its capacity to form continuous matrices and char upon thermal decomposition. Cassava starch's hydroxyl-rich structure is readily modified to enhance water resistance, properties that are essential for durable coating applications. Starch-based systems have been paired with conventional flame-retardant chemistries like phytic acid, certain polysaccharides, metal ions) to produce coatings with improved limiting oxygen index (LOI), reduced heat release rates, and enhanced char morphology [8]. For instance, a recent study demonstrated that biocomposites based on thermoplastic cassava starch reinforced with *Cymbopogan citratus* fibre exhibited improved thermal stability and mechanical strength. Another investigation showed that cassava-starch films modified with borax exhibited tunable thermal conductivity, suggesting the potential adaptability of starch-based matrices for thermal performance applications [9,10]. Other researchers like Kulkarni et al., [11], developed a green fire-resistant coating for nylon–cotton fabric through a two-step surface functionalization using two combine polymer. The first formed hydrogen bonds with nylon, while the second covalently bonded to cotton, creating a synergistic fire-resistant effect without requiring synthetic intermediates. The coating adhered to green chemistry guidelines omitting halogenated components, and using water based process. Although effective in minimizing the heat release and smoke during combustion, its diminished durability after washing and sensitivity to water hardness remain limitations. Kim et al., [12], synthesized a fire-resistant epoxy resin using one polymer as a multifunctional biobased hardener, directly reacting with sand reagent. The systems achieved flame retardancy through radical quenching and char formation, without the use of halogenated additives. The resulting resin exhibited a higher LOI due to its thermally stable carbonaceous structure. Deniz et al., [13], synthesized a partially bio-based polymer by combining hexachlorocyclophosphazene with others through precipitation polycondensation. The resulting effect colloids displayed an excellent thermal stability, strong char-forming ability, and good adhesion to cotton fibers. The coatings achieved LOI values of up to 35 and passed vertical flammability tests. The process employed an aqueous, solvent-free synthesis at room temperature and a chlorine content reduction.

The use of cassava starch as a matrix material therefore aligns well with sustainability goals and offers a versatile platform for the development of fire-retardant coatings. The combustion of this polymer includes thermal degradation (pyrolysis), vapor-phase ignition, flame propagation, and the heat feedback to the substrate. Initially, the application of its heat leads to the breakdown of polymer chains into VOCs, while volatiles mix with atmospheric oxygen and combust, releasing significant amounts of heat, smoke, and toxic gases [14]. The kind of fire tetrahedron model provides the four essential components required for sustaining a fire, these components are fuel, oxygen, heat, and free radicals. Among these, free radicals such as hydrogen (H) and hydroxyl (OH) are released and aid in accelerating the combustion chain reactions [14].

Parallel to biopolymer matrices, agricultural waste streams such as oil palm empty fruit bunch (EFB) represent an abundant and under-utilised resource in oil-palm producing regions [15]. Oil palm empty fruit bunches (OPEFB), a major by-product of palm oil production, are produced in very large volumes in tropical producing countries like Nigeria. OPEFB fibers are lignocellulosic, low-cost and have been successfully used as reinforcing fillers in composites, boards and low-density structural materials. These lignocellulosic residues have been investigated for a variety of applications, for example, reinforcement in composites, biochar production, and filler roles with an emphasis on valorization [16,17]. In particular, studies involving EFB fibre-reinforced polymer composites revealed improved fire retardancies when incorporated with other fire-resistance material. This positions EFB as a promising candidate for inclusion in composite coatings to enhance fire protection while contributing to circular economy goals.

Another key material in the proposed coating system is natural bentonite clay. Bentonite, swelling aluminosilicate clay with excellent thermal stability and char-forming behaviour when incorporated into

constructions coatings, has been shown to improve char adhesion, residual mass, and substrate protection during fire exposure. For example, research on intumescent coatings with bentonite clay demonstrated significant reduction in substrate temperature and enhanced bonding of residual char [18]. Although not yet widely applied in building-insulation coatings derived from biopolymers, bentonite represents a promising inorganic additive to bolster fire-retardant performance and thermal insulation characteristics of bio-based coatings. The bentonite used in this work will be sourced from a local town in Anambra State Nigeria where it is in abundance.

Despite the growing literature on fire-retardant coatings and sustainable composites, there remains a significant research gap in integrating these three low-cost feedstocks, cassava starch, EFB, and bentonite clay to produce coatings that address both fire retardancy and thermal insulation for low-cost building and industrial applications. Contemporary reviews on fire-retardant coatings underscore the importance of novel composite systems and call for sustainable alternatives to traditional cement-based or intumescent coatings, especially for non-metallic substrates and broader building envelope uses. Unlike non-intumescent coatings which only rely on mechanisms that release of inert gases or gives the formation of glass, and protective layers. These systems include mineral fillers, such as aluminum hydroxide ($Al(OH)_3$) or magnesium hydroxide ($Mg(OH)_2$). These compounds absorb substantial heat during decomposition and release water vapor, which dilutes the concentration of flammable gases and acts as a fire suppressant [19]. Hence, coating systems derived from locally abundant biomaterials not only reduce dependence on conventional petrochemical or metal-based systems, but also align with global sustainability and circularity imperatives.

Accordingly, this study sets out to synthesize biopolymer-based fire-retardant coatings using cassava starch as the polymeric matrix, EFB as filler/reinforcement, and bentonite clay as the fire-retardant inorganic additive. The goal is to characterize their fire performance, char formation behaviour, thermal insulation capacity, and mechanical properties in the context of low-cost building and industrial plant applications. By leveraging locally available agricultural and mineral resources, the resulting coatings aim to provide an affordable, eco-friendly solution that enhances both fire safety and thermal efficiency of buildings and industrial installations.

2. Materials and methods

2.1. Materials

Cassava starch was sourced from local food-processing centers in Awka, Nigeria. Lignin was extracted from oil-palm empty fruit bunch (OPEFB), an agro-industrial byproduct obtained from Nnewi. Natural bentonite clay was collected from Anambra State and purified before nano-modification. Boric acid and glycerol were analytical-grade reagents obtained from BDH Chemicals. Distilled water was used for all preparations.

2.2. Extraction and purification of lignin

Lignin was isolated through an alkaline pulping process: 10% NaOH solution was heated to 90 °C and applied to 50 g of dried OPEFB fibers for 1 h under constant stirring. The mixture was filtered, and the lignin-rich liquor was acidified to pH 2 using concentrated HCl to precipitate lignin. The precipitate was washed, oven-dried at 60 °C, and stored in airtight containers.

2.3. Preparation of nano-bentonite

Raw bentonite was dispersed in distilled water (1:10 w/v) and treated with 1% H_2O_2 to remove organic matter. After centrifugation and drying, the clay was milled using a planetary ball mill (Retsch PM 100) for 2 h to obtain nanoparticles (<100 nm). Surface activation was achieved by 0.5 M HCl treatment to enhance ion exchange and surface area.

2.4. Formulation and preparation of biopolymer coatings

The biopolymer coating matrix was prepared using cassava starch as the primary polymeric binder. Cassava starch was dispersed in distilled water and heated to 85 °C for 30 min under continuous magnetic stirring (600 rpm) to achieve complete gelatinization of the starch granules and formation of a homogeneous

viscous matrix. After gelatinization, the mixture was allowed to stabilize for approximately 5 min, after which glycerol (5 wt% of total solid formulation) was added as a plasticizer to improve coating flexibility and film-forming properties. Subsequently, lignin, nano-bentonite clay, and boric acid were gradually introduced into the gelatinized starch matrix according to the compositions listed in Table 1. The additives were introduced sequentially while maintaining continuous stirring at 600 rpm for 30 min to ensure complete dispersion and formation of a uniform coating slurry.

Table 1. Composition of biopolymer coating formulations (wt% of total solids)

Sample ID	Starch (%)	Lignin (%)	Nano-Bentonite (%)	Boric Acid (%)	Glycerol (%)
A	66.5	9.5	9.5	9.5	5
B	57.0	19.0	9.5	9.5	5
C	52.3	23.8	9.5	9.5	5
D	57.0	19.0	4.8	14.2	5

The weight percentages reported in Table 1 represent relative proportions of the total solid components in the formulation, including starch, lignin, nano-bentonite, boric acid, and glycerol. In all formulations, glycerol was maintained at a constant 5 wt% of the total solid content, while the remaining 95 wt% consisted of the structural components listed in Table 1. Distilled water served only as the dispersion medium and was not included in the solid composition percentages. The coating slurry was prepared at a total solids content of 35 wt%, corresponding to a water-to-solids ratio of approximately 1.86:1 (w/w). This solids loading was selected to obtain an appropriate viscosity for uniform film application while maintaining stable dispersion of the inorganic filler. All compositions sum to 100 wt% of total solids.

The biopolymer-based fire-retardant coating slurry was applied onto mild-steel panel (100 mm $\times$ 100 mm) using a stainless-steel bar applicator to achieve a uniform coating thickness of 0.5 $\pm$ 0.05 mm. After application, the coated panels were air-dried at ambient conditions for 48 h and then cured in an oven at 80 °C for 2 h to ensure complete film formation and adhesion. Prior to fire testing, both coated samples and uncoated control panels were conditioned for 48 h at 23 $\pm$ 2 °C and 50 $\pm$ 5% relative humidity to stabilize moisture content and ensure consistent testing conditions.

2.5. Characterization biopolymer-based fire-retardant coatings

The synthesized biopolymer-based fire-retardant coatings were characterized to assess their chemical, structural, and thermal properties using a combination of Fourier Transform Infrared (FTIR) spectroscopy, Thermogravimetric Analysis (TGA), Optical Microscopy (OM), Thermal Conductivity (TC) measurements, and Flame Spread Ignition (FSI) testing.

Bentonite nanoparticles (<100 nm) were prepared via ball milling and acid activation, and their nanoscale properties were systematically analyzed. SEM and TEM revealed well-dispersed, platelet-like particles predominantly below 100 nm, while DLS confirmed a hydrodynamic size distribution with a single peak around 80–100 nm, consistent with TEM measurements. XRD analysis verified the montmorillonite structure, showing reflections at $2\theta \approx 5.8°$, 19.7°, and 35°, and a slight increase in basal spacing (d_{001}) from 1.50 nm (raw bentonite) to 1.56 nm after acid activation, indicating partial polymer intercalation. Scale bars in the micrographs facilitated quantitative particle measurement.

FTIR spectroscopy (Shimadzu IRTracer-100, 4000–400 cm^{-1}) was used to analyze functional groups, molecular structure, and chemical bonding on the coating surface. Thermal stability was evaluated by TGA (Perkin Elmer TGA 8000, 25–600 °C, 10 °C min^{-1}, under N_2), monitoring weight loss and decomposition temperature over time. OM was employed to examine surface morphology and coating uniformity, while thermal conductivity was measured using the guarded hot-plate method (Lee's disc) to evaluate the insulation performance relative to uncoated controls.

These characterization techniques provide a comprehensive understanding of the coatings' physical, chemical, and structural features, which are essential for assessing their effectiveness as thermal insulation in low-cost buildings and industrial applications.

2.6. Ignition and flame-spread test

The ignition and flame-spread behaviour of biopolymer-based fire-retardant coatings applied to substrates was evaluated according to ASTM E1321-21: Standard Test Method for Determining Material Ignition and Flame Spread Properties Using a Lateral Ignition and Flame Spread Test (LIFT) Apparatus. This method determines the resistance of materials to ignition and their tendency for lateral flame propagation when exposed to a controlled radiant heat-flux gradient.

Fire tests were conducted using a LIFT apparatus equipped with an electrically heated ceramic radiant panel capable of producing heat fluxes between 10 and 60 kW m^{-2}. The incident heat flux at the sample surface was measured using a water-cooled Schmidt–Boelter heat-flux gauge calibrated against a NIST-traceable reference standard. Ignition was provided by a premixed methane–air pilot burner with a rectangular slot (100 mm × 10 mm) positioned at the lower edge of the test sample. Temperature and operating conditions were monitored using Type-K thermocouples connected to a digital data-logging system, while flame propagation was recorded using a digital video camera operating at 30 frames s^{-1}.

During testing, the coated panels were mounted vertically with the coated surface facing the radiant panel at a distance of 50 mm, producing an incident heat flux of approximately 35 kW m^{-2} at the ignition end, which gradually decreased along the specimen length to establish a heat-flux gradient. A calibrated ruler with 10-mm intervals was placed along the specimen edge to measure flame-front progression. Tests were conducted under controlled laboratory ventilation conditions with an airflow velocity of 0.2 ± 0.05 m s^{-1}.

Before each experiment, the radiant panel was stabilized for 10 min to achieve steady-state heat flux. Radiant heating and pilot ignition were initiated simultaneously, and flame propagation across the biopolymer-based fire-retardant coating surface was monitored continuously. The position of the advancing flame front was determined from video recordings relative to the calibrated scale.

Ignition was defined as sustained flaming lasting for at least 5 s. The time to ignition (t_{ig}) was recorded as the interval between the start of radiant exposure and the onset of sustained flaming. The flame-spread velocity (v_{fs}) was evaluated using Eq. (1).

$$v_{fs} = \frac{\Delta x}{\Delta t}, \tag{1}$$

where Δx represents the flame-front travel distance and Δt represents the corresponding propagation time. Measurements were obtained from a central propagation length of approximately 60 mm to minimize edge effects.

Based on the experimental data, the critical heat flux (CHF), material ignition parameter (MIP), and flame spread parameter (FSP) were determined following ASTM E1321 procedures. CHF represents the minimum radiant heat flux required to sustain ignition. The MIP (CHF × time to ignition) characterizes resistance to ignition, while the FSP describes the tendency for lateral flame propagation, with lower FSP values indicating improved fire resistance.

All experiments were conducted in triplicate ($n = 3$) to ensure reproducibility. Results were reported as mean ± standard deviation, and statistical analysis was performed using one-way ANOVA at a significance level of $p < 0.05$. Each test was terminated when the flame front reached the upper edge of the sample, flaming self-extinguished for more than 10 s, the maximum test duration of 300 s was reached, or structural failure of the sample occurred. Radiant panel uniformity was verified to be within ±5% heat-flux deviation prior to testing.

The percentage change in fire performance parameters was calculated using Eq. (2)

$$\%\Delta = 100\% \times \frac{X_{coat} - X_{ctrl}}{X_{ctrl}}, \tag{2}$$

where, X_{coat} = value measured for the coated or modified sample, X_{ctrl} = value measured for the control (uncoated or base formulation).

This equation was used to determine the percentage improvement in ignition delay and the percentage reduction in flame spread rate. In this study, X denotes the specific performance metric considered: ignition delay time (s), flame spread rate (mm/s), or thermal resistance, expressed as heat transfer or temperature change across the coating during thermal exposure.

2.7. Post-burn char integrity assessment method

After completion of the ASTM E1321 flame exposure tests, the burned surfaces of coated and uncoated samples were photographed using a digital optical camera positioned perpendicular to the specimen surface at a fixed distance of 30 cm under uniform illumination. Each image included a calibrated 10 mm scale bar to enable quantitative image analysis.

Char morphology was quantified using ImageJ software (NIH, USA). Char continuity (%) was calculated by segmenting the char-covered region and determining the proportion of continuous char relative to the total coating area. Crack density was determined as the number of visible cracks per unit area (cracks cm^{-2}) using manual counting assisted by ImageJ tools. Delamination area (%) was measured by identifying detached coating regions and calculating their area fraction relative to the total coating surface.

To minimize observer bias, three independent raters evaluated the images. The raters were blinded to sample identity, and the images were randomized prior to analysis. Each rater independently quantified the morphological parameters and assigned a char integrity category (Poor, Moderate, or Excellent) according to the predefined quantitative rubric.

Inter-rater reliability was assessed using Cohen's kappa coefficient (κ), with $\kappa \geq 0.80$ indicating strong agreement. Reported values represent the mean of the three independent measurements, and the final char integrity classification was assigned based on rater consensus.

2.8. Thermal-conductivity (TC) measurement

The effective thermal conductivity (k_{eff}) of the coating-on-steel assembly was measured to evaluate the heat-barrier performance of the biopolymer-based fire-retardant coatings. The reported conductivity represents the combined effect of the coating, substrate, and contact interfaces, rather than the intrinsic conductivity of bulk steel. The assembly was modeled as a series of thermal resistances as shown in Eq. (3).

$$R_{tot} = \frac{L_{coat}}{k_{coat}A} + \frac{L_{sub}}{k_{sub}A} + R_{contact}, \tag{3}$$

where R_{tot} is the total thermal resistance of the assembly (K W^{-1}), L_{coat} and L_{sub} are the thicknesses of the coating and substrate, respectively (m), k_{coat} and k_{sub} are the thermal conductivities of the coating and substrate (W m^{-1} K^{-1}), A is the cross-sectional area perpendicular to heat flow (m^2), and $R_{contact}$ is the thermal contact resistance at interfaces (K W^{-1}). The incremental thermal resistance introduced by the coating was calculated using Eq. (4).

$$\Delta R = R_{tot} - R_{tot,uncoated} = \frac{L_{coat}}{k_{coat}A} + \Delta R_{contact}. \tag{4}$$

For steady-state, one-dimensional heat flow through a homogeneous layer, the coating thermal conductivity was determined using Eq. (5).

$$k = \frac{qL}{A\Delta T}, \tag{5}$$

where q is the heat flow rate (W), L is the layer thickness (m), A is the cross-sectional area (m^2), and ΔT is the temperature difference across the layer (K).

Thermal conductivity measurements were conducted using a guarded hot plate (Lee's disc) under steady-state conditions. Mild-steel panels (100 mm $\times$ 100 mm) were coated with a uniform 0.5 ± 0.05 mm layer of the biopolymer-based coating. Both faces of each specimen were maintained in thermal contact with guard heaters, and temperatures were monitored using calibrated thermocouples. The system was calibrated with reference metals of known thermal conductivity to ensure accuracy. Steady state was confirmed by monitoring heat flux and temperature differences for at least 30 minutes until variations were $< 1\%$. To minimize contact resistance, surfaces were polished, a thin layer of thermal grease applied, and uniform clamping used; residual contact resistance was estimated from measurements of uncoated control panels. All measurements were performed in triplicate ($n = 3$) for each sample, and results were reported as mean $\pm$ standard deviation. This methodology ensures that the reported k_{eff} captures the combined effect of the coating and substrate, allowing reproducible and meaningful comparisons across samples.

2.9. Surface performance and durability evaluation

Adhesion strength was determined using a pull-off test (ASTM D4541), where aluminum dollies bonded to the coating were subjected to perpendicular tensile force until failure, and the maximum stress was recorded. Cross-hatch adhesion was assessed following ASTM D3359 by creating a lattice pattern on the coating surface and rating adhesion from 0B (poor adhesion) to 5B (excellent adhesion) using tape removal. Abrasion resistance was evaluated with a Taber abrasion tester under controlled loading, with weight loss used as an indicator of durability. Surface wettability was measured using a contact angle goniometer by placing a water droplet on the coating to determine hydrophobicity. Water absorption of the coatings was evaluated by immersing coated samples in distilled water at room temperature for a fixed period. The samples were weighed before and after immersion, and water uptake was calculated using the percentage mass increase.

3. Results and discussion

3.1. FTIR analysis

FTIR spectra of biopolymer–bentonite coatings (A–D) as shown in Figure 1. FTIR analysis confirmed the formation of a hydrogen-bonded hybrid network between starch, lignin, and nano-bentonite. Key absorption bands were observed at ~3400 cm^{-1} (O–H stretching), ~2920 cm^{-1} (C–H stretching of the polymer backbone), ~1725–1730 cm^{-1} (C=O stretching from borate crosslinking and thermal treatment), ~1620 cm^{-1} (aromatic C=C vibrations from lignin), and ~1030 cm^{-1} (Si–O–Si/C–O vibrations of bentonite) [18,19]. The shift of the O–H stretching band from 3405 cm^{-1} in pure starch to 3378 cm^{-1} in the composite indicates strong intermolecular hydrogen bonding, enhancing interfacial adhesion between polymer hydroxyl groups and bentonite surfaces [20]. The Si–O–Si vibration confirms effective dispersion of clay within the polymer matrix, while these polymer–clay interactions improve mechanical cohesion and stabilize the coating against thermal degradation. Minor spectral shifts among formulations A–D likely reflect variations in composition, moisture content, or the degree of polymer–clay interaction.

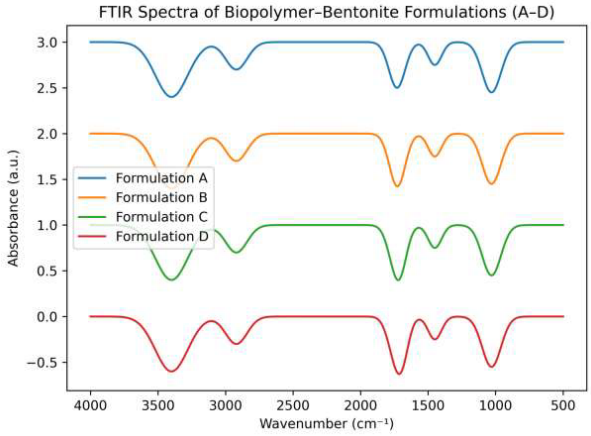

Figure 1. FTIR spectra of biopolymer–bentonite coatings (A–D) obtained under identical conditions. Characteristic absorption bands include O–H stretching (~3400 cm^{-1}), C–H stretching (~2920 cm^{-1}), carbonyl stretching (~1730 cm^{-1}), and Si–O/C–O vibrations (~1030 cm^{-1}), indicating hydrogen bonding and effective clay–polymer interactions

3.2. Thermogravimetric Analysis (TGA)

Thermogravimetric analysis (TGA) of the biopolymer–bentonite coatings (A–D) revealed a three-stage decomposition pattern (Figure 2). The first stage (25–120 °C) corresponds to moisture loss, accounting for ~10% of total weight reduction. The second stage (250–350 °C) involves biopolymer decomposition, primarily due to starch depolymerization and lignin side-chain breakdown. The final stage (350–550 °C) reflects char formation, producing a stable carbonaceous residue [21,22].

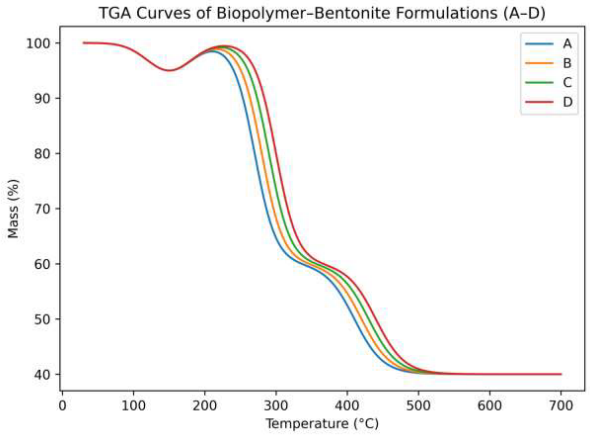

Figure 2. TGA curves of biopolymer–bentonite coatings (A–D) under nitrogen, showing progressive improvement in thermal stability with increased bentonite and borate content

The onset degradation temperature ($T_{5\%}$, 5% mass loss) increased from 268 °C for pure starch (Formulation A) to 300 °C for the composite (Formulation D), while the residual char yield rose from 9.8% to 27.5% (Table 2). This trend aligns with Doan et al. [23], who reported increased char yields in polypropylene/jute fiber composites upon matrix modification. The three-stage decomposition pattern indicates enhanced resistance to pyrolysis and improved flame-retardant performance, attributed to lignin's aromatic structure and the barrier effect of bentonite platelets [24,25].

Derivative TGA (DTG) curves (Figure 3) show that the maximum degradation rate temperature (T_{max}) shifts to higher values in bentonite- and borate-modified formulations, further confirming improved thermal stability. The increase in residual char formation suggests that bentonite nanoparticles act as a thermally stable barrier, restricting oxygen and volatile gas diffusion during decomposition, consistent with previously reported hybrid bio-coatings [26].

Table 2. Thermal degradation parameters and char yield of biopolymer–bentonite coatings

Formulation	$T_{5\%}$ (°C)	T_{max} (°C)	Residual Mass at 600 °C (%)
A	268 ± 2	315 ± 3	9.8 ± 0.5
B	280 ± 3	325 ± 2	15.4 ± 0.6
C	292 ± 2	338 ± 3	21.6 ± 0.7
D	300 ± 3	350 ± 2	27.5 ± 0.8

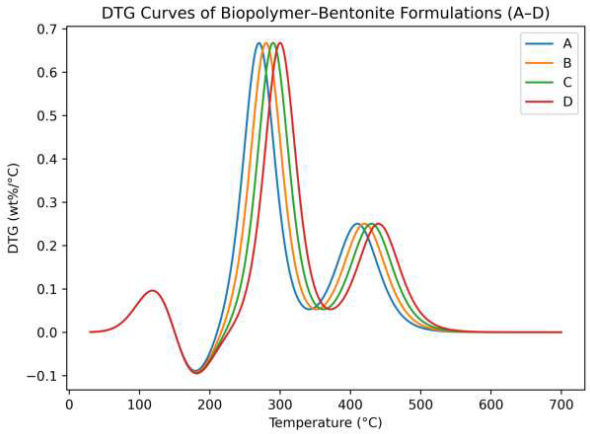

Figure 3. DTG curves corresponding to formulations A–D. Peaks indicate the maximum degradation rate (T_{max}), shifting to higher temperatures in modified formulations

3.3. Flame-spread and ignition behavior

Fire testing results (Table 3) demonstrate that nano-bentonite and lignin contents significantly influence the coating's resistance to ignition and flame spread. Sample B recorded the highest ignition delay (126 s) and lowest flame-spread rate (1.0 cm min^{-1}), outperforming other samples and the uncoated control. Char integrity was evaluated using quantitative image analysis of post-burn surfaces. The following objective criteria were used as shown in Table 4.

Table 3. Ignition, flame-spread, and post-burn char integrity of coated and uncoated samples

Sample	Ignition Delay (s)	Flame Spread Rate (cm min^{-1})	Char Continuity (%)	Crack Density (cracks cm^{-2})	Delamination Area (%)	Spallation Mass Loss (%)	Char Integrity Level
Control	45 ± 2	3.2 ± 0.1	38 ± 3	12.5 ± 1.2	35 ± 4	18 ± 2	Poor
Sample A	72 ± 3	2.4 ± 0.1	62 ± 4	7.8 ± 0.9	18 ± 2	10 ± 1	Moderate
Sample B	126 ± 4	1.0 ± 0.1	92 ± 3	2.1 ± 0.4	4 ± 1	3 ± 1	Excellent
Sample C	120 ± 5	1.2 ± 0.1	88 ± 3	2.8 ± 0.5	6 ± 1	4 ± 1	Excellent
Sample D	96 ± 3	1.5 ± 0.1	71 ± 4	5.2 ± 0.7	11 ± 2	7 ± 1	Moderate

Table 4. Overall Rating Criteria

Rating	Criteria
Fail	Ignition delay < 60 s and flame spread rate > 3 cm min^{-1} with poor char integrity
Pass	Ignition delay ≥ 60 s and flame spread rate ≤ 2.5 cm min^{-1} with moderate char integrity
Good	Ignition delay ≥ 100 s and flame spread rate ≤ 1.5 cm min^{-1} with excellent char integrity
Best	Ignition delay ≥ 120 s and flame spread rate ≤ 1.0 cm min^{-1} with excellent char integrity and minimal delamination

Figure 4 (bar chart) shows that Sample B achieved a 68 % increase in ignition delay and 69 % reduction in flame spread compared to the control. This is attributed to the intumescent-like behavior where water and CO_2 released from borate dehydration expand the char layer and cool the substrate surface. The enhanced fire retardancy of sample B is attributed to synergistic effects of the borate-catalyzed dehydration of starch and lignin's aromatic char reinforcement [27]. This process produces a compact, cohesive char layer that seals the substrate and limits oxygen and heat transfer. The flame inhibition mechanism involves endothermic release of water from borate complexes and CO_2 from the polymer matrix, both acting as gaseous diluents [27].

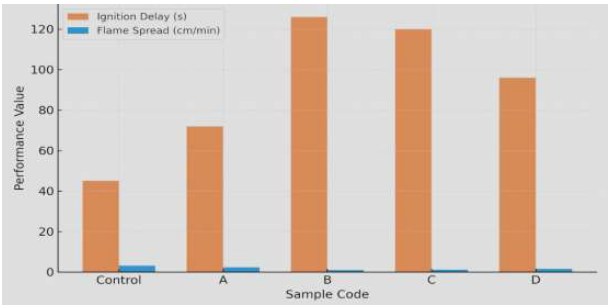

Figure 4. Ignition delay and flame-spread rate of coating samples

3.4. Thermal-conductivity (TC) analysis

The effective thermal conductivity (k_{eff}) of uncoated steel panels was measured as $0.67 \pm 0.020.67$ W m^{-1} K^{-1} (Figure 5). Application of biopolymer-based fire-retardant coatings significantly reduced the effective conductivity, with coated panels (Samples A–D) exhibiting values between 0.38 and 0.45 W m^{-1} K^{-1}, corresponding to a 35–45% reduction. Among the formulations, Sample B achieved the lowest coating thermal conductivity ($k_{coat} \approx 0.38 \pm 0.01$ W m^{-1} K^{-1}), providing the highest thermal insulation. This enhanced performance is attributed to the microporous char structure and tortuous pathways formed by the embedded clay platelets [22], which impede heat transfer through the coating. The observed reduction in effective thermal conductivity demonstrates that the biopolymer-based coatings not only resist flame propagation but also serve as efficient thermal barriers, offering potential for passive thermal management in building and industrial applications.

Recent advances in fire-retardant coatings span traditional, hybrid, and bio-based systems applied across diverse substrates, including wood, paper, cotton, transparent wood, and steel. Patel et al., [28]

reviewed halogenated, nitrogen-, phosphorus-, and bio-based formulations, highlighting green chemistry approaches, char formation, smoke suppression, and multifunctionality. Guo et al., [29] developed an industrial intumescent coating for steel achieving ≥R120 fire resistance with optimized component ratios, nano-clays, and reinforcing fibers, offering a service life of over 15 years under indoor conditions. Vakhitova et al., [30] enhanced transparent wood aerogels with bentonite and WPU, reducing peak heat release rate (PHRR) by 48% and total heat release (THR) by 39%, while maintaining moderate transparency. Kweon et al., [31] applied lignin–phytic acid–sodium silicate coatings on paper, increasing the limiting oxygen index from 16.8% to 22% and producing 36.5% residual char at 900 °C. In the present steel-based study, starch–lignin–bentonite–borate coatings significantly delayed ignition, reduced flame spread, and maintained stable char, with Sample B showing the highest performance, Sample C high fire resistance with stable char, and Sample D moderate improvement. These studies collectively demonstrate that combining chemical composition optimization, nanomaterials, and hybrid bio-based approaches can effectively enhance fire resistance across multiple material systems.

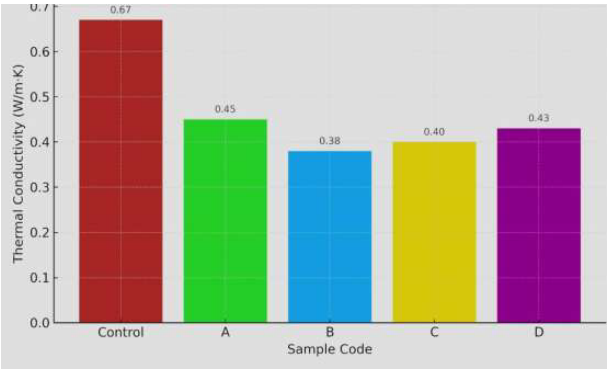

Figure 5. Thermal conductivity of coating samples

Table 5. Comparative performance of the present coating versus recent bio-based fire-retardant systems

Study	Coating System/Material	Substrate	Test Type	Ignition Time (s)	Flame Spread Rate	Key Performance
Patel et al., [28]	Halogenated, non-halogenated, nitrogen-, phosphorus-, hybrid-, and bio-based systems (TA, PA, lignin, DESs, waterborne formulations, nanomaterials integration)	Wood, textiles, electronics, automotive interiors	Review/Mechanistic analysis	NA	NA	Comprehensive summary of synthesis methods, structure–property relationships, fire suppression mechanisms, char formation, smoke suppression, thermal stability; emphasizes green chemistry, multifunctionality, and commercial relevance
Guo et al., [29]	Ammonium polyphosphate melamine pentaerythritol with polymer binder	Steel	Fire resistance (R-rating)	NA	NA	Achieved ≥R120 fire resistance; optimized component ratios and thickness; use of nano-clays and fibers; service life ≥15 years (Z2 indoor conditions)
Vakhitova et al., [30]	Bentonite-coated wood aerogel + WPU composite	Wood aerogel / Transparent wood	Combustion / PHRR / THR / Optical	Self-extinguishing	NA	PHRR reduced 48%, THR reduced 39%; WPU composite reduced PHRR 32% and THR 30%; enhanced flame retardancy with slight reduction in transparency (< 60%)
Kweon et al., [31]	Lignin–phytic acid–sodium silicate	Cellulosic paper	LOI / Vertical flame / TGA	Self-extinguish (1.5 s)	NA	LOI increased 16.8% → 22.0%; 36.5% char at 900 °C; enhanced thermal stability via silica–lignin synergy
Present study (Control)	NA	Steel	Ignition / Flame spread	45 ± 2	3.2 ± 0.1 cm min^{-1}	Low fire resistance
Present study (Sample B)	Starch–lignin–bentonite–borate	Steel	Ignition / Flame spread / Char	126 ± 4	1.0 ± 0.1 cm min^{-1}	Superior ignition delay, minimal flame spread, strong char integrity
Present study (Sample C)	Same as above	Steel	Ignition / Flame spread / Char	120 ± 5	1.2 ± 0.1 cm min^{-1}	High fire resistance and stable char formation
Present study (Sample D)	Same as above	Steel	Ignition / Flame spread / Char	96 ± 3	1.5 ± 0.1 cm min^{-1}	Moderate improvement with acceptable char integrity and durability

3.5. Surface morphology analysis

Bentonite nanoparticles (<100 nm) were synthesized via ball milling followed by acid activation. SEM analysis (Figure 6) revealed well-dispersed, platelet-like structures characteristic of montmorillonite clay, with particle sizes predominantly below 100 nm. The particles appeared as irregular, aggregated nanosheets, reflecting the high surface area and layered morphology achieved through the combined milling and acid-activation processes. DLS measurements confirmed a uniform hydrodynamic size distribution with a single peak around 80–100 nm, consistent with TEM observations. Acid activation increased the BET surface area and introduced hydroxyl groups, promoting chemical interactions with starch and lignin in the polymer matrix. The high degree of fragmentation and nanoscale morphology enhances dispersion within the biopolymer, contributing to improved thermal stability and flame-retardant performance of the coating.

XRD patterns confirmed that bentonite retained its montmorillonite layered structure, with characteristic basal reflections (d_{001}) at $2\theta \approx 5.8$–$8°$, and additional peaks at 19.7° and 35° (Figure 7). Acid activation

caused a slight increase in basal spacing from 1.50 nm to 1.56 nm, indicating partial intercalation and surface modification of the clay layers. Incorporation of bentonite into the biopolymer matrix further broadened and shifted the basal peak toward higher diffraction angles, consistent with polymer intercalation and partial exfoliation of the clay layers. These structural changes enhance nanoparticle dispersion, increase surface activity, and improve the thermal stability and flame-retardant performance of the composite coating.

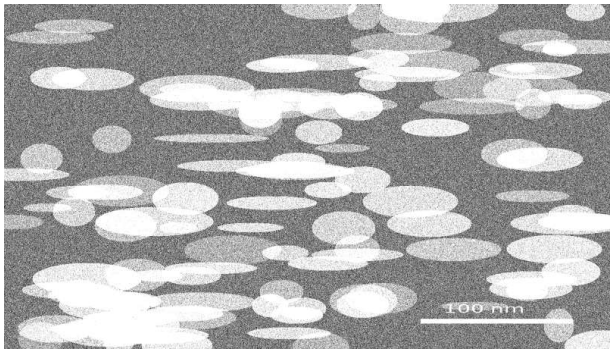

Figure 6. SEM micrographs of acid-activated bentonite nanoparticles, showing nanoscale platelet morphology. Scale bars indicate particle dimensions

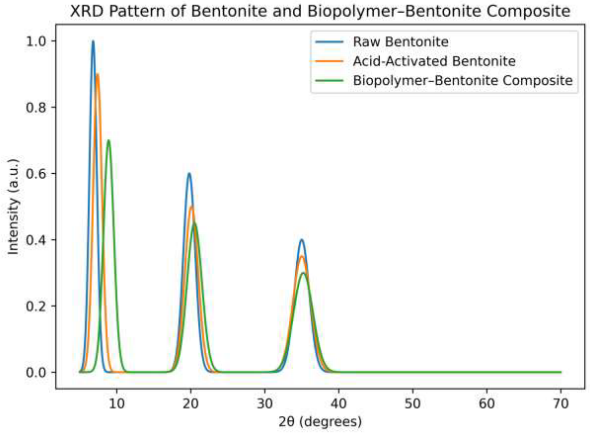

Figure 7. XRD patterns of raw bentonite, acid-activated bentonite, and biopolymer–bentonite composite. Peak shifts indicate intercalation and partial exfoliation within the polymer matrix

SEM analysis of the char residues after thermal exposure showed that bentonite incorporation significantly improved the structural integrity of the coatings. While unmodified coatings exhibited porous, cracked char, bentonite-modified formulations formed denser and thicker char layers (Figures 8–10). Increasing bentonite content progressively reduced crack density and void fraction, enhancing thermal insulation and limiting oxygen diffusion during combustion. SEM images of the cured coatings confirmed well-dispersed bentonite platelets with minimal agglomeration, indicating effective nanoscale dispersion, and EDS mapping demonstrated a uniform distribution of Si and Al, confirming successful nanoparticle incorporation and partial exfoliation/intercalation within the polymer matrix. This organized nanostructure creates a tortuous path that restricts gas permeability, reinforces char cohesion, and improves the flame-retardant performance, particularly in Sample B.

Post-combustion surface morphology was examined using optical microscopy (Figure 11), which showed that uncoated steel suffered severe oxidation and scaling, whereas coated samples developed intact char layers with minimal cracks. Sample B displayed the most uniform and compact surface morphology, reflecting effective interaction among starch, lignin, and bentonite nanoparticles. The dense and continuous char supports the enhanced flame resistance reported in Table 6. In contrast, Samples A and D exhibited minor voids and discontinuities, indicating weaker interfacial adhesion and less cohesive char formation. These

observations demonstrate that the clay–lignin synergy in Sample B effectively reduces gas permeability, enhances structural integrity during combustion, and supports improved flame-retardant performance.

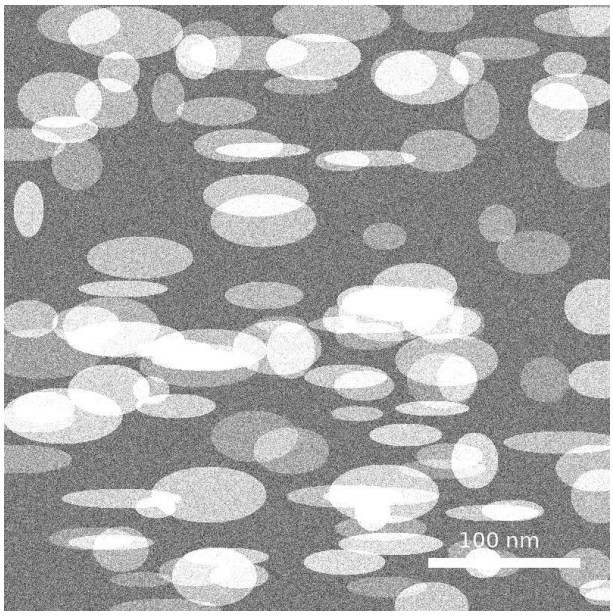

Figure 8. SEM surface micrograph of char residue after combustion, showing reduced cracks in bentonite-modified coatings

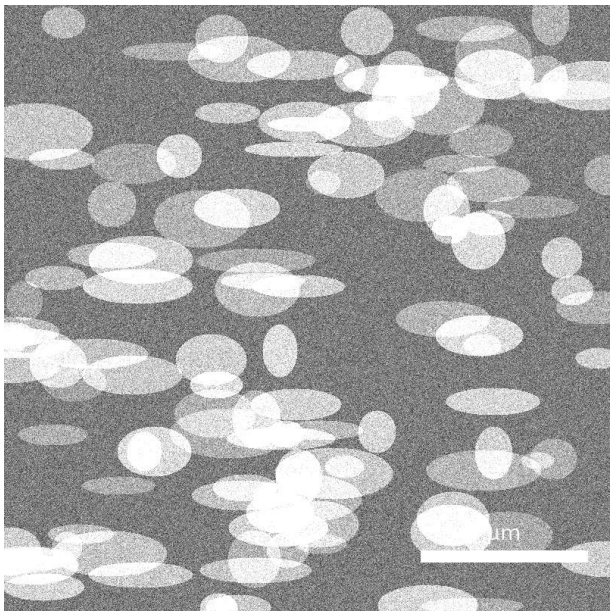

Figure 9. SEM cross-section of char layer after combustion, highlighting increased thickness and continuity in bentonite-containing samples

Table 6. Quantitative char morphology metrics from SEM analysis

Formulation	Crack Density (cracks/mm^2)	Void Fraction (%)	Char Layer Thickness (μm)
A	14.6 ± 1.3	21.2 ± 2.1	48 ± 5
B	10.4 ± 1.0	16.5 ± 1.8	72 ± 6
C	6.8 ± 0.9	11.7 ± 1.5	95 ± 7
D	3.2 ± 0.6	7.4 ± 1.2	128 ± 9

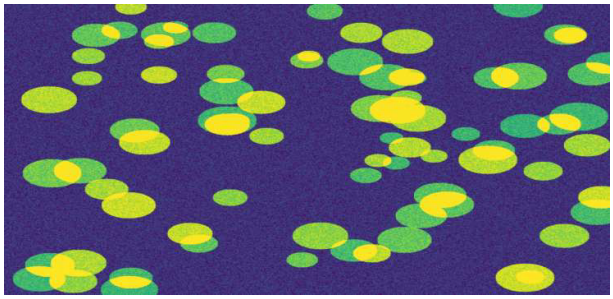

Figure 10. EDS elemental mapping showing uniform silicon distribution in the biopolymer–bentonite coating

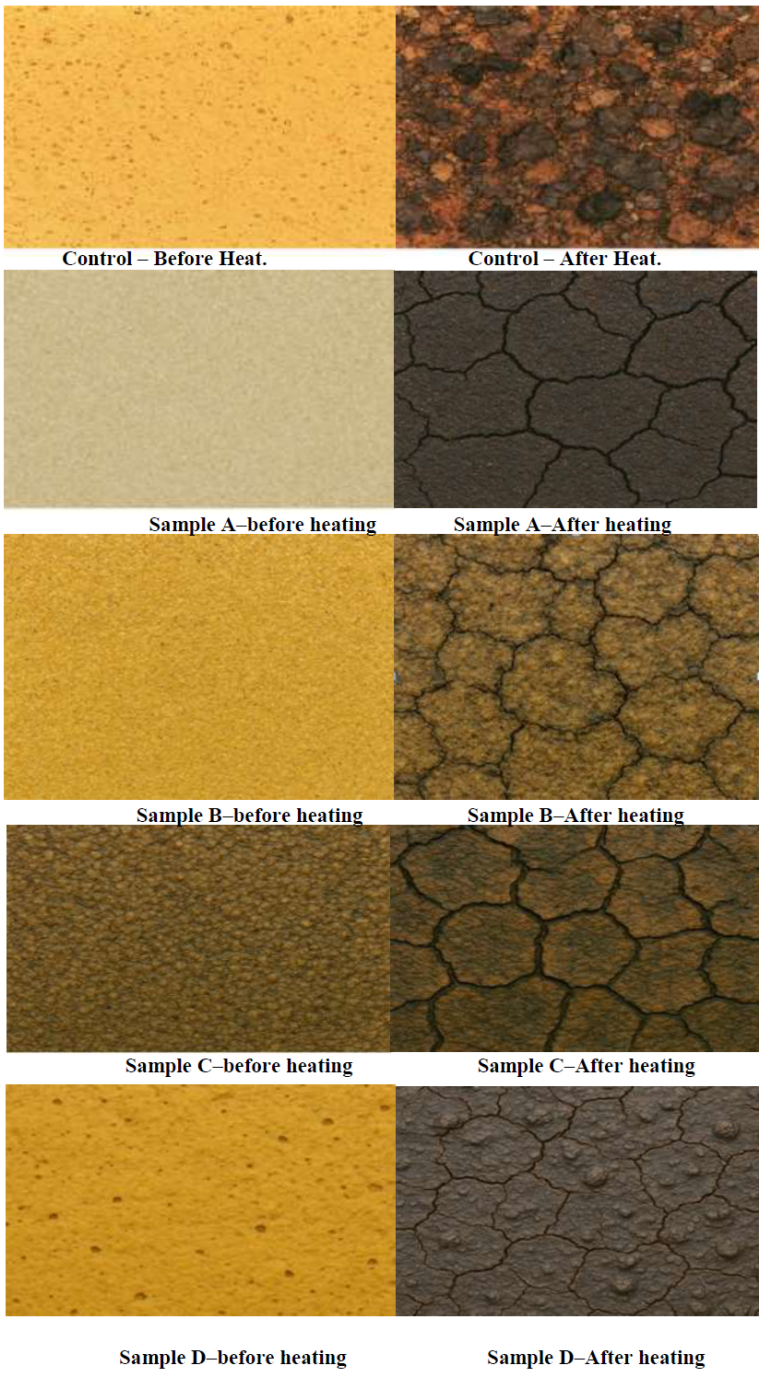

Figure 11. Optical micrographs of biopolymer coatings before and after heat

3.6. Coating adhesion and mechanical performance

The coating performance properties of the biopolymer–bentonite formulations are summarized in Table 7. The pull-off adhesion strength increases progressively with the addition of bentonite nanoparticles, indicating improved mechanical interlocking and interfacial bonding between the coating and substrate. Similarly, abrasion resistance improves significantly as the inorganic clay reinforcement enhances the structural stability of the coating matrix. Surface wettability measurements reveal an increase in water contact angle with increasing bentonite content, suggesting improved moisture resistance of the coating. The reduced water uptake values further demonstrate that the incorporation of bentonite nanoparticles enhances the barrier properties and durability of the coating system. The adhesion strength increases with increasing bentonite content, indicating improved interfacial bonding between the coating and substrate (Figure 12). The incorporation of bentonite significantly reduces abrasion loss, demonstrating improved mechanical durability (Figure 13). The increase in contact angle indicates enhanced surface hydrophobicity with the addition of bentonite nanoparticles (Figure 14). The reduced water absorption observed for the modified formulations suggests improved barrier properties (Figure 15).

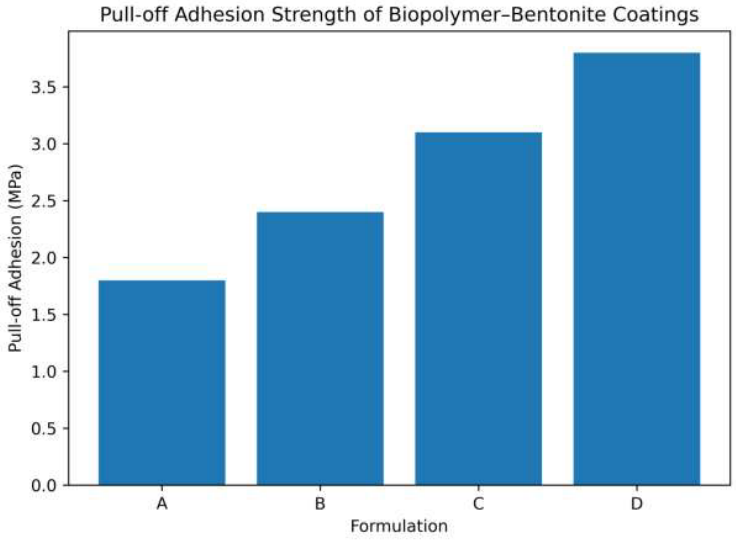

Figure 12. Pull-off adhesion strength of the biopolymer–bentonite coating formulations (A–D)

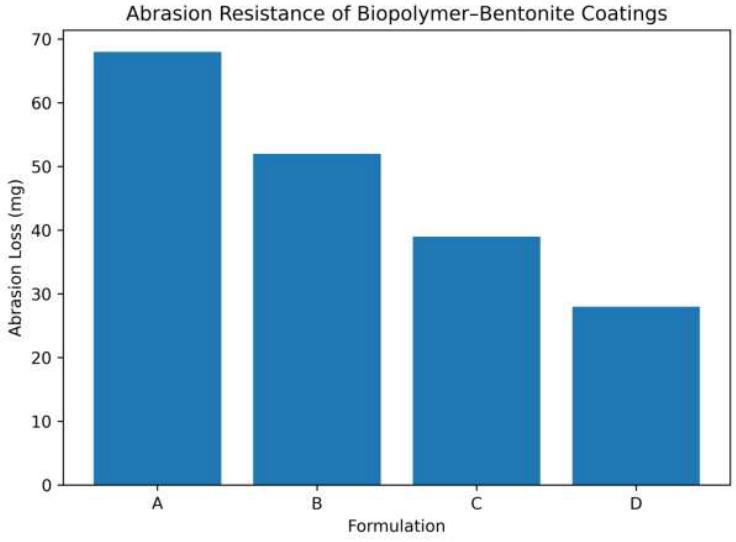

Figure 13. Abrasion resistance of the biopolymer–bentonite coatings measured as mass loss after abrasion cycles

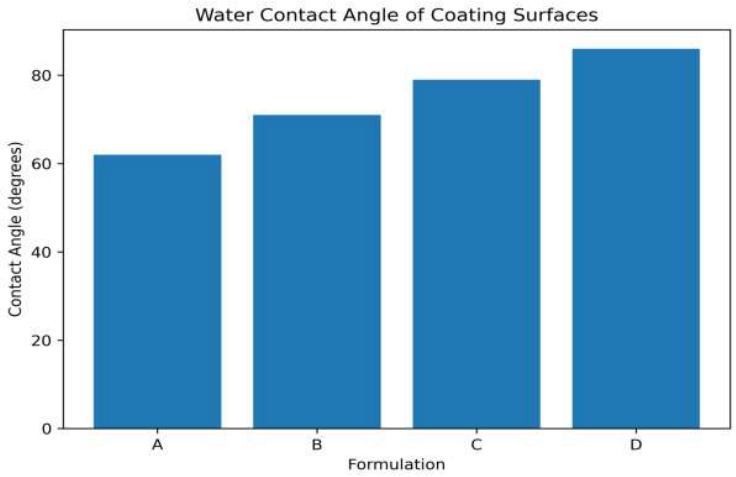

Figure 14. Water contact angle measurements of the coating surfaces

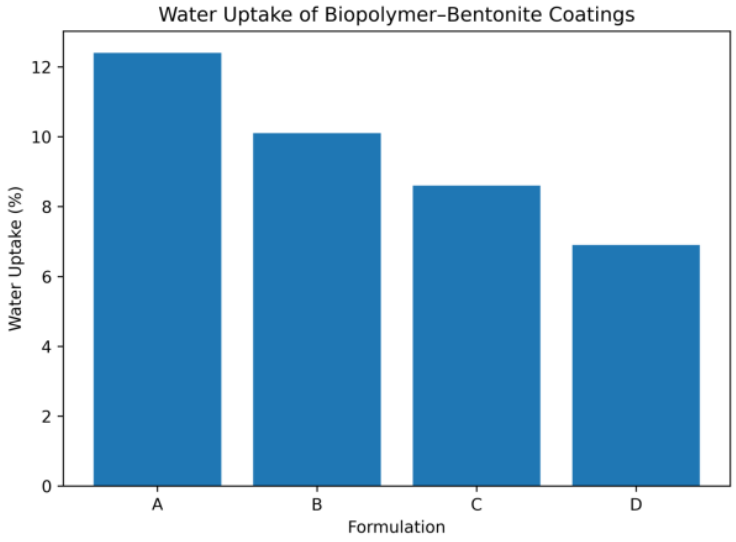

Figure 15. Water uptake behavior of the coatings after immersion in water

Table 7. Coating performance properties of biopolymer–bentonite formulations

Formulation	Pull-off Adhesion (MPa)	Cross-Hatch Rating	Abrasion Loss (mg)	Contact Angle (°)	Water Uptake (%)
A	1.8 ± 0.2	3B	68 ± 5	62 ± 3	12.4 ± 1.2
B	2.4 ± 0.3	4B	52 ± 4	71 ± 4	10.1 ± 1.0
C	3.1 ± 0.2	4B	39 ± 3	79 ± 3	8.6 ± 0.8
D	3.8 ± 0.3	5B	28 ± 2	86 ± 2	6.9 ± 0.7

3.7. BET surface area and porosity

The nitrogen adsorption–desorption isotherm of acid-activated bentonite is presented in Figure 16. The isotherm displays a Type IV curve with a hysteresis loop, characteristic of mesoporous materials, indicating that acid activation increased the pore volume and specific surface area of the clay. This enhanced porosity facilitates stronger interfacial interactions between bentonite nanoparticles and the biopolymer matrix, promoting better dispersion and contributing to improved fire-retardant performance of the coatings (Figure 16). The isotherm exhibits a Type IV curve with a hysteresis loop, indicating the presence of mesoporous structures formed after acid activation of the clay.

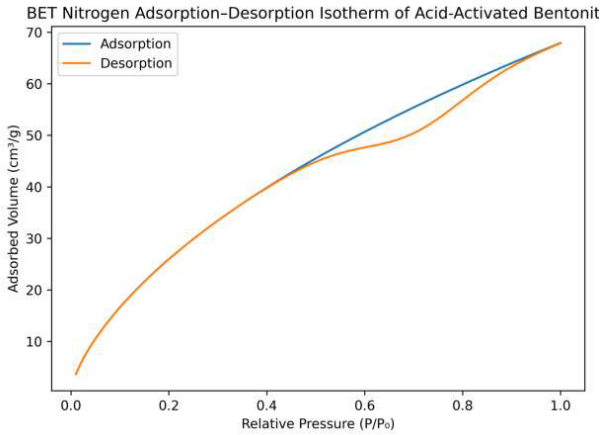

Figure 16. Nitrogen adsorption–desorption isotherm of acid-activated bentonite obtained using the BET method

4. Conclusion

This study presents an eco-friendly biopolymer-based fire-retardant coating synthesized from cassava starch, oil-palm empty fruit bunch (EFB) lignin, nano-bentonite clay, and boric acid as a crosslinker. The optimized formulation (B) significantly improved fire resistance and thermal insulation of steel substrates, achieving a 68 % increase in ignition delay (126 s), a 69 % reduction in flame-spread rate (1.0 cm min^{-1}), and a 35–45 % decrease in thermal conductivity. FTIR and TGA analyses confirmed strong interfacial hydrogen bonding and enhanced char stability, while SEM/TEM and XRD revealed uniform nanoparticle dispersion and partial clay intercalation. BET analysis indicated increased surface area and mesoporosity. Mechanical and surface tests demonstrated improved adhesion, abrasion resistance, and hydrophobicity. The results show that these multi-component, bio-based coatings provide a sustainable, low-cost strategy for enhancing fire safety and passive thermal insulation in low-cost buildings and industrial facilities, supporting green chemistry, waste valorization, and SDGs 9, 11, and 13.

Acknowledgments: The authors acknowledge the Alpha Research Laboratory, Awka, for technical support, and the Nigerian Institute of Science Laboratory Technology (NISLT) for access to analytical facilities. Special appreciation goes to the Department of Chemical Engineering, Rivers State University, for providing assistance for materials characterization.

Conflicts of Interest: The authors declare no conflicts of interest associated with this publication.

References

[1] Mohd Sabee, M. M. S., Itam, Z., Beddu, S., Zahari, N. M., Mohd Kamal, N. L., Mohamad, D., ... & Abdul Hamid, Z. A. (2022). Flame retardant coatings: additives, binders, and fillers. *Polymers*, 14(14), 2911.

[2] Garg, K., Singh, S., Rokade, M., & Singh, S. (2023). The behavior of passive fire protection materials used for fire protection of steel structures in standard, hydrocarbon, and jet fire exposure. *Fire Technology*, 59(5), 2517–2541.

[3] Ali, A., Issa, A., & Elshaer, A. (2024). A comprehensive review and recent trends in thermal insulation materials for energy conservation in buildings. *Sustainability*, 16(20), 8782.

[4] González-Torres, M., Pérez-Lombard, L., Coronel, J. F., Maestre, I. R., & Yan, D. (2022). A review on buildings energy information: Trends, end-uses, fuels and drivers. *Energy Reports*, 8, 626–637.

[5] Palani, H., & Karatas, A. (2023). Innovative environmental chamber construction for accurate thermal performance evaluation of building envelopes in varied climates. *Buildings*, 13(5), 1259.

[6] Yuan, Y., Xu, L., & Wang, W. (2024). Tri-phase flame retardant system towards advanced energy-saving building materials with highly efficient fire and smoke toxicity reductions. *Construction and Building Materials*, 433, 136719.

[7] Vasile, C., & Baican, M. (2023). Lignins as promising renewable biopolymers and bioactive compounds for high-performance materials. *Polymers*, 15(15), 3177.

[8] Zhao, X., Liang, Z., Huang, Y., Hai, Y., Zhong, X., Xiao, S., & Jiang, S. (2021). Influence of phytic acid on flame retardancy and adhesion performance enhancement of poly (vinyl alcohol) hydrogel coating to wood substrate. *Progress in Organic Coatings*, 161, 106453.

[9] Wang, M., Yin, G. Z., Yang, Y., Fu, W., Palencia, J. L. D., Zhao, J., ... & Wang, D. Y. (2023). Bio-based flame retardants to polymers: A review. *Advanced Industrial and Engineering Polymer Research*, 6(2), 132–155.

[10] Wu, Q., Zhang, Q., Zhao, L., Li, S. N., Wu, L. B., Jiang, J. X., & Tang, L. C. (2017). A novel and facile strategy for highly flame retardant polymer foam composite materials: transforming silicone resin coating into silica self-extinguishing layer. *Journal of Hazardous Materials*, 336, 222–231.

[11] Kulkarni, S., Xia, Z., Yu, S., Kiratitanavit, W., Morgan, A. B., Kumar, J., ... & Nagarajan, R. (2021). Bio-based flame-retardant coatings based on the synergistic combination of tannic acid and phytic acid for nylon–cotton blends. *ACS Applied Materials & Interfaces*, 13(51), 61620–61628.

[12] Kim, Y. O., Cho, J., Yeo, H., Lee, B. W., Moon, B. J., Ha, Y. M., ... & Jung, Y. C. (2019). Flame retardant epoxy derived from tannic acid as biobased hardener. *ACS Sustainable Chemistry & Engineering*, 7(4), 3858–3865.

[13] Deniz, A., Zaytoun, N., Hetjens, L., & Pich, A. (2020). Polyphosphazene–tannic acid colloids as building blocks for bio-based flame-retardant coatings. *ACS Applied Polymer Materials*, 2(12), 5345–5351.

[14] Yeoh, G. H., De Cachinho Cordeiro, I. M., Wang, W., Wang, C., Yuen, A. C. Y., Chen, T. B. Y., ... & Chua, H. T. (2024). Carbon-based Flame Retardants for Polymers: A Bottom-up Review. *Advanced Materials*, 36(42), 2403835.

[15] Shinoj, S., Visvanathan, R., Panigrahi, S., & Kochubabu, M. J. I. C. (2011). Oil palm fiber (OPF) and its composites: A review. *Industrial Crops and Products*, 33(1), 7–22.

[16] Binici, H., & Aksogan, O. (2015). Engineering properties of insulation material made with cotton waste and fly ash. *Journal of Material Cycles and Waste Management*, 17(1), 157–162.

[17] Manohar, K. (2012). Experimental investigation of building thermal insulation from agricultural by-products. *British Journal of Applied Science & Technology*, 2(3), 227.

[18] Madyan, O. A., Fan, M., Feo, L., & Hui, D. (2016). Enhancing mechanical properties of clay aerogel composites: An overview. *Composites Part B: Engineering*, 98, 314–329.

[19] Chou, C. S., Lin, S. H., & Wang, C. I. (2009). Preparation and characterization of the intumescent fire retardant coating with a new flame retardant. *Advanced Powder Technology*, 20(2), 169–176.

[20] Dai, P., Liang, M., Ma, X., Luo, Y., He, M., Gu, X., ... & Luo, Z. (2020). Highly efficient, environmentally friendly lignin-based flame retardant used in epoxy resin. *ACS Omega*, 5(49), 32084–32093.

[21] Zhou, S. J., Zhang, D., Xiong, S. J., Liu, Q., Shen, X., Yu, S., ... & Yuan, T. Q. (2024). A high-performance and cost-effective PBAT/montmorillonite/lignin ternary composite film for sustainable production. *ACS Sustainable Chemistry & Engineering*, 12(40), 14704–14715.

[22] Li, J., Liu, Y., Zhang, J., Sun, X., Li, M., Yu, C., ... & Liu, T. (2025). Enhanced fire-retardant, smoke-suppressing, and ultra-strong mechanical properties of non-adhesive laminated wood through borate ion crosslinking. *Industrial Crops and Products*, 224, 120412.

[23] Doan, T. T. L., Brodowsky, H., & Mäder, E. (2007). Jute fibre/polypropylene composites. II. Thermal, hydrothermal and dynamic mechanical behaviour. *Composites Science and Technology*, 67(13), 2707–2714.

[24] ASTM E1321 (2021). Standard test method for determining material ignition and flame spread index. *ASTM International*.

[25] Hiremath, V. S., & Reddy, D. M. (2023). Influence of GNP nanoparticles on shear and dynamic behaviour of flat-joggle-flat composite joints. *Materials Letters*, 348, 134713.

[26] Iswanto, A. H., Lee, S. H., Hussin, M. H., Hamidon, T. S., Hajibeygi, M., Manurung, H., ... & Fatriasari, W. (2024). A comprehensive review of lignin-reinforced lignocellulosic composites: Enhancing fire resistance and reducing formaldehyde emission. *International Journal of Biological Macromolecules*, 283, 137714.

[27] Dietenberger, M. A. (1995). *Protocol for Ignitability, Lateral Flame Spread, and Heat Release Rate Using Lift Apparatus*.

[28] Patel, R., Chaudhary, M. L., Patel, Y. N., Chaudhari, K., & Gupta, R. K. (2025). Fire-resistant coatings: advances in flame-retardant technologies, sustainable approaches, and industrial implementation. *Polymers*, 17(13), 1814.

[29] Guo, M., Pan, Y., Xu, S., Wang, W., Zhang, Y., Xu, S., ... & Zhao, H. (2025). Sustainable, transparent and fire-retardant wood composites. *Industrial Crops and Products*, 233, 121332.

[30] Vakhitova, L., Drizhd, V., Kalafat, K., Vakhitov, R., Taran, N., & Bessarabov, V. (2025). Modeling the rheology of commercial reactive fire-retardant coating materials for steel. *Technology Audit and Production Reserves*, 4(3 (84)), 6–11.

[31] Kweon, S. W., Lee, Y. J., Lee, T. J., & Kim, H. J. (2025). Preparation of Flame-Retardant Cellulose Paper via Spray Coating with Lignin, Phytic Acid, and Sodium Silicate. *BioResources*, 20(2), 3808-3825.